Resonant Raman scattering by LO phonons in $Al_xGa_{1-x}As$ ($x < 0.1$): Alloying and interference effects

W. Kauschke, M. Cardona, and E. Bauser
Max-Planck-Institut für Festkörperforschung, Heisenbergstrasse 1, Postfach 80 06 65, D-7000 Stuttgart 80, Federal Republic of Germany
(Received 31 December 1986)

The resonant Raman scattering by LO and two LO phonons and LO-phonon interference effects are studied near the $E_0+\Delta_0$ gap of liquid-phase-epitaxy $Al_xGa_{1-x}As$ ($0 \leq x \leq 0.07$) samples at 100 K. The $E_0+\Delta_0$ gap is shifted and broadened due to the alloying, whereas the interference between dipole-allowed and dipole-forbidden Raman scattering persists. Within the composition range studied the $E_0+\Delta_0$ gap as well as its Lorentzian broadening η depends linearly on the alloy composition x [$E_0+\Delta_0(x)=1.847+1.56x$ eV, $\eta(x)=3.8+120x$ meV]. Estimates for the η-versus-x behavior based on a simple tight-binding model and on binominal statistics for a random distribution of Al atoms on Ga sites do not explain the alloy broadening observed for the $E_0+\Delta_0$ gap. Inhomogeneous broadening due to clustering fluctuations in x or other crystal defects cannot be discarded. The measured absolute values of the corresponding Raman efficiencies agree well with calculated ones. The comparison between the different $Al_xGa_{1-x}As$ samples shows that aluminum in GaAs does not significantly enhance the impurity-induced dipole-forbidden Raman scattering by LO phonons.

I. INTRODUCTION

The ternary III-V semiconductor system $Al_xGa_{1-x}As$ has important optoelectronic applications and its electronic properties have, therefore, been extensively studied. The compositional dependence of the lowest direct and indirect band gaps was determined by many optical methods such as absorption,[1-5] reflectance,[6] electroreflectance,[7,8] and ellipsometry[9] (for a review see Ref. 10). The main interest has been focused on the direct gap E_0 at the Γ point (Γ_8^v-Γ_6^c), on the indirect gap between the X and Γ points (Γ_8^v-X_6^c), and on the crossover of the conduction-band minimum at the X and Γ points occurring for $x \simeq 0.45$. A nonlinear dependence of the band gaps on alloy composition x was observed, which was confirmed, for the E_0 gap, by photoluminescence measurements.[5,11,12]

Band-structure calculations for mixed-crystal systems aim at explaining the dependence of the band gaps on composition. They concentrate on the deviation from the linear dependence, the so-called band bowing. Most of the band-structure calculations for the $Al_xGa_{1-x}As$ system use the virtual-crystal approximation[13,14] (VCA) in which the cation potential is replaced by a weighted average of the Ga and Al potentials. The VCA alone leads either to a linear compositional dependence of the E_0-band gap or, with some modifications, to a very small bowing parameter.[15,16] Disorder effects, such as broadening due to alloy scattering, are neglected in this approximation, since the electronic states are supposed to be undamped ($\mathbf{k}$ to be a good quantum number). They can be partially included by the coherent-potential approximation[17,18] (CPA) which considers the effect of scattering caused by potential fluctuations around the average potential due to the random distribution of Ga and Al atoms (positional disorder). Alloy scattering limits, e.g., the electron and hole mobility in ternary and quaternary semiconductors.[12] The crystal potential can be decomposed into a periodic part [scaled virtual-crystal approximation (SVCA)] and an aperiodic part that takes the random deviations from the scaled virtual-crystal behavior into account.[19,20] The random potential is assumed to be site diagonal. The CPA requires large computational work, since it includes integrations over the Brillouin zone. It yields the self-energies of the electronic states whose real parts account for the shift of the electronic states caused by alloy scattering, whereas the imaginary parts are related to the finite lifetime. The CPA has been applied to band-structure calculations of alloy semiconductors using the pseudopotential,[15-17,21] $\mathbf{k}\cdot\mathbf{p}$,[18] and tight-binding (TB) method.[19,20,22-24] Real-space approaches such as tight-binding calculations have some advantage, since CPA assumes the alloy disorder to be site diagonal. The TB method, however, represents the conduction-band states less accurately than the valence-band states. Nevertheless, in the case of the E_0 gap, it yields in connection with the CPA, positive bowing parameters as found experimentally in $Al_xGa_{1-x}As$ and small alloy broadenings.[19,24] On the other hand, the CPA neglects effects of compositional disorder such as clustering. The existence of short- and long-range order in $Al_xGa_{1-x}As$ has, however, been proved experimentally[25,26] and its influence on the alloy properties theoretically discussed.[27,28]

The study of the vibrational properties of $Al_xGa_{1-x}As$ alloys by infrared and Raman spectroscopy revealed a two-mode behavior of the long-wavelength longitudinal and transverse optical phonons throughout nearly the whole composition range (for $x<0.8$ GaAs-like and for $x>0.08$ AlAs-like modes).[29-33] For sufficiently high aluminum concentrations ($x \simeq 0.43$) the second-order spectrum shows, besides the second harmonics of the GaAs- and AlAs-like LO modes, their combination.[31,33]

The low-energy part of the Raman spectra contains disorder-activated longitudinal- (DALA) and transverse-acoustical modes (DATA).[33–36] The line profiles of the GaAs- and AlAs-like LO phonons depend on composition and are asymmetrically broadened by disorder.[33]

In this paper we focus our attention on the resonant Raman scattering by LO phonons near the $E_0+\Delta_0$ gap in $Al_xGa_{1-x}As$ on the Ga-rich side of the composition range ($x<0.1$). The Raman scattering by LO phonons occurs via a short-range and a long-range part of the electron-phonon interaction.[37–39] Analytic expressions for the resonance of Raman scattering by LO phonons near the $E_0+\Delta_0$ gap due to the different scattering mechanisms have been derived previously and successfully applied to interpret experiments on GaAs,[40,41] $Cd_xHg_{1-x}Te$,[42] InP,[43] and GaSb.[44]

The deformation-potential-induced Raman scattering is of short range and obeys usual dipole selection rules.[37–39] It resonates weakly near $E_0+\Delta_0$, since no two-band terms are operative at this gap.[38,46] The long-range interaction arises from the Fröhlich electron-phonon coupling via the electric field of the LO phonon in polar semiconductors.[37–39] The *interband* Fröhlich coupling contributes to the dipole-allowed Raman scattering (electrooptic mechanism), whereas the *intraband* Fröhlich interaction leads to the dipole-forbidden (**q**-dependent) Raman scattering by LO phonons. The latter appears for the polarization of the incident and scattered light parallel to each other and resonates close to all direct gaps, when the energy of the incident light equals the gap plus half the phonon energy ($\hbar\omega_L=E_g+\frac{1}{2}\hbar\Omega_{LO}$).[43] The phonon wave vector **q** is determined in this first-order Raman process by the difference between the wave vector of the incident and scattered light $\mathbf{k}_{L,S}$ ($\mathbf{q}=\mathbf{k}_L-\mathbf{k}_S$). The scattering efficiency for **q**-induced Raman scattering resonates with strengths proportionally to q^2.[47–50]

A second mechanism is operative for the dipole-forbidden Raman scattering by LO phonons. It assumes the electron-hole pair created by the electron-photon interaction to be scattered by the Fröhlich electron-phonon interaction[51–53] and also by the interaction (usually Coulomb) with impurities. In spite of low impurity concentrations and fourth-order perturbation expressions, the impurity-induced Raman scattering may be significant, since the elastic scattering by ionized impurities activates LO phonons with large **q** vectors and double resonances occur (the **q** conservation is relaxed).[41,43] The impurity-induced Raman scattering by LO phonons exhibits "incoming" ($\hbar\omega_L=E_g$) and "outgoing" resonances ($\hbar\omega_L=E_g+\hbar\Omega_{LO}$), the latter being in general stronger.[43]

The resonance of second-order Raman scattering by LO phonons is formally similar to that of the impurity-induced scattering by one LO phonon. A second Fröhlich interband electron-phonon interaction has to replace the electron-impurity interaction in the fourth-order perturbation expression.[42,43,54–59] The resonance of two-LO-phonon Raman scattering reveals a sharp distinct peak at the outgoing resonance ($\hbar\omega_L=E_g+2\hbar\Omega_{LO}$).[43] The resonance profile of scattering by two LO phonons has been shown to provide accurate values for the energy and broadening of the $E_0+\Delta_0$ gap in $Cd_xHg_{1-x}Te$ (Ref. 42) and InP (Ref. 43). In the case of $Cd_xHg_{1-x}Te$ ($p\simeq10^{16}$ cm^{-3}), the shift of dipole-forbidden Raman scattering by one LO phonon with respect to the two-LO-phonon resonance ($\Delta E\simeq h\Omega_{LO}$) suggests that the one-LO-phonon scattering is mainly impurity induced.[42] On the other hand, the dipole-allowed and intrinsic dipole-forbidden Raman scattering by one LO phonon have been shown to interfere in high-purity epitaxial GaAs (Refs. 40 and 41) and InP (Ref. 43). The interference is less pronounced in bulk GaSb (Ref. 44) ($n\simeq10^{15}$ cm^{-3}) and bulk GaAs (Ref. 41) ($n=10^{15}$ cm^{-3}). This feature follows from the fact that the Raman tensor for deformation-potential-induced dipole-allowed and intrinsic **q**-induced dipole-forbidden scattering must be coherently added *before* squaring to obtain the scattering intensity. The extrinsic impurity-induced Raman scattering adds as intensity to the intrinsic mechanisms *after* squaring. The relative strength of the intensity due to the intrinsic and extrinsic dipole-forbidden Raman scattering by LO phonons can be obtained by fitting the measured resonance profiles for the interference and dipole-forbidden scattering simultaneously with analytic expressions for the different Raman scattering mechanisms presented in Refs. 41–43. In epitaxial samples of GaAs and InP the intrinsic **q**-induced scattering by LO phonons contributes only about 40% to the dipole-forbidden scattering intensity.[42,43] In the case of InP, excellent agreement between the experimental data and the fitted curves has been obtained by starting the fitting procedure from accurate values for the $E_0+\Delta_0$ gap and its broadening determined from the two-LO-phonon-resonance, since the Raman scattering by one LO phonon is rather insensitive to both parameters.[43] This procedure has not yet been applied to GaAs.

In this paper we present additional data for the resonance of two-LO-phonon scattering and, on their basis, revise the fits of Ref. 41 for GaAs. Especially the broadening parameter η of the $E_0+\Delta_0$ gap has to be decreased from 8 to about 3.5 meV. We will focus our attention to the alloy system $Al_xGa_{1-x}As$. The observation of the resonance of Raman scattering by two LO phonons allows us to study the variation of the gap position and its broadening with alloy composition x. The interference of Raman scattering by one LO phonon is very sensitive to broadening and also to impurity scattering. Although the gap shifts and broadens due to alloy disorder we find that the interference persists in the alloys for Raman scattering by one phonon. The Al atom, isoelectronic to Ga, perturbs the band states much less than the ionized impurities considered in the theory of impurity-induced Raman scattering. Two estimates are given for the dependence of the gap broadening on x. The predicted broadenings are too low. Inhomogeneous broadening may account for the additional observed width.

II. EXPERIMENTAL PROCEDURE

Four high-purity $Al_{1-x}Ga_xAs$ samples covering the aluminum content $0\leqq x<0.1$ were investigated. They are n-type undoped epitaxial layers grown on a semi-insulating GaAs(001) substrate by liquid-phase epitaxy (LPE). The aluminum content x was estimated from the

bound-exciton luminescence at liquid-helium temperature using the dependence of the direct gap $E_0(x)$ at Γ (Γ_8^v-Γ_6^c) on x:[11]

$$E_0(x)=1.515+1.247x \text{ eV } (0<x\leqq 0.45) . \quad (1)$$

The $x=0$ gap was shifted from 1.424 eV to 1.515 eV in order to account for a temperature shift of 295 K and the shift of the direct gap E_0 with respect to the bound-exciton line.[60] Equation (1) does not include the dependence of the bound-exciton energy on x.[61] Table I summarizes the characteristics of the different samples: the Al concentration obtained from the $E_0(x)$ luminescence [Eq. (1)], the mobility at 77 K, and the estimated concentration of ionized impurities $n_{77\,K}\simeq N_D-N_A$ deduced from Hall measurements.

With increasing x the mobility decreases. It remains, however, above values reported for Czochralski-grown bulk GaAs.[41] Besides the alloy scattering which reduces the electron mobility,[12] the increasing impurity concentration with increasing aluminum content may be due to residual oxide films on the aluminum added to the melt. They have been (partially) removed by etching before adding the aluminum to the melt. The quality and the homogeneity of the samples was checked by looking for below-band-gap luminescence, such as electron-acceptor transitions.[62]

The measurements were performed in backscattering geometry on a (001) surface. We denote by x, y, z, x', and y' the [100], [010], [001], [110], and [$\bar{1}$10] directions, respectively. For the labeling of the [110] and [$\bar{1}$10] directions we refer to the convention of Ref. 41 [Ga at the origin, As at $a_0/4$ (1,1,1)]. With this definition the ($\bar{1}1\bar{1}$) plane (parallel to [110]) is Ga terminated. The etch pattern produced by preferential etching of the (001) face distinguished between the [110] and [$\bar{1}$10] directions.[63]

For backscattering at a (001) face the Raman tensor of the scattering by LO phonons can be written as follows.

(i) Dipole-allowed scattering via deformation-potential interaction:[38,64]

$$\overleftrightarrow{R}_{DP}=\begin{pmatrix} 0 & a_{DP} & 0 \\ a_{DP} & 0 & 0 \\ 0 & 0 & 0 \end{pmatrix} . \quad (2)$$

(ii) q-induced dipole-forbidden scattering via Fröhlich interaction:[38,41]

$$\overleftrightarrow{R}_{F}=\begin{pmatrix} a_F & 0 & 0 \\ 0 & a_F & 0 \\ 0 & 0 & a_F \end{pmatrix} . \quad (3)$$

(iii) Impurity-induced dipole-forbidden scattering via Fröhlich interaction:[41]

$$\overleftrightarrow{R}_{Fi}=\begin{pmatrix} a_{Fi} & 0 & 0 \\ 0 & a_{Fi} & 0 \\ 0 & 0 & a_{Fi} \end{pmatrix} . \quad (4)$$

a_{DP}, a_F, and a_{Fi} are the corresponding Raman polarizabilities.

The deformation-potential and the q-induced Fröhlich scattering by LO phonons are intrinsic processes which lead to the same final states in q space. They are mutually coherent. Thus, their Raman tensors have to be added *before* squaring to yield the Raman scattering intensity $|\hat{e}_S\cdot\overleftrightarrow{R}\cdot\hat{e}_L|^2$ [$\hat{e}_L(\hat{e}_S)$ denotes the polarization vector of the incident (scattered) light]. The impurity-induced Fröhlich scattering is incoherent, since it leads to a manifold of final states in q space. Its scattering *intensity* has to be added to that of intrinsic processes. By measuring in four different backscattering configurations we can distinguish between the scattering processes mentioned above. The squared Raman polarizabilities $|\hat{e}_S\cdot\overleftrightarrow{R}\cdot\hat{e}_L|^2$ are as follows:[41]

$$\begin{aligned} &\text{(I) } \bar{z}(x',x')z, \\ &\quad |a_F+a_{DP}|^2+|a_{Fi}|^2 . \\ &\text{(II) } \bar{z}(y',y')z, \\ &\quad |a_F-a_{DP}|^2+|a_{Fi}|^2 . \\ &\text{(III) } \bar{z}(x,x)z, \\ &\quad |a_F|^2+|a_{Fi}|^2 . \\ &\text{(IV) } \bar{z}(y,x)z, \\ &\quad |a_{DP}|^2 . \end{aligned} \quad (5)$$

Three rectangular slabs were cut from each sample and mounted next to each other in a liquid-nitrogen cryostat. The vertical axes corresponded to the [110], [$\bar{1}$10], and [100] directions, so that the measurements in configurations I–III could be performed by parallel translation of the samples with respect to the entrance slit of the monochromator without changing the polarization of the incident light. The Raman scattering by two LO phonons was investigated in configuration III. The polarization of the incident light was changed for the measurement of the dipole-allowed Raman scattering by LO phonons in configuration IV.

Pure silicon was chosen as a reference to obtain abso-

TABLE I. Samples characteristics.

	Sample 1	2	3	4
Al concentration (at. %)	0	1.7±0.3	3.3±0.3	7.0±0.5
$E_0(x)$ (eV) at 4 K	1.515	1.538	1.556	1.603
$\mu_{77\,K}$ (cm^2/V s)	100 000	41 400	19 500	13 100
$n_{77\,K}$ (cm^{-3})	7×10^{12}	3.4×10^{14}	5.8×10^{14}	3.2×10^{15}

lute values for the Raman scattering efficiencies $dS/d\Omega$ and the squared Raman tensors $|\hat{e}_S\cdot\vec{R}\cdot\hat{e}_L|^2$ by the sample substitution method.[38] We used $|a_{Si}|=40$ Å for the optical phonon of silicon at $\hbar\omega_L=1.9$ eV.[65] We took a small dispersion of the Raman polarizability of Si over the whole spectral range 1.8–2.1 eV into account.[66]

The counting rate *outside* the crystal R_S' is related to the squared Raman polarizability *inside* the crystal by[41]

$$R_S'=\left[\frac{T_S T_L \omega_S^3[n(\Omega_{ph})+1]}{(\alpha_L+\alpha_S)n_S n_L M^*\Omega_{ph}V_c}\right]\frac{P_L'\Delta\Omega'}{2c^4}|\hat{e}_S\cdot\vec{R}\cdot\hat{e}_L|^2 . \tag{6}$$

P_L' is the incident power, and $\Delta\Omega'$ is the collection solid angle *outside* the crystal. α_L (α_S), n_L (n_S), and T_L (T_S) denote the absorption coefficient, refractive index, and transmission coefficient at the frequency ω_L (ω_S) of the incident (scattered) light, respectively, c is the speed of the light in vacuum, $M^*=[1/(M_{Ga}(1-x)+M_{Al}x)+1/M_{As}]^{-1}$ the reduced mass of the primitive cell with volume V_c, and $n(\Omega_{ph})$ the phonon occupation number of the optical phonon with frequency Ω_{ph}. In the case of Raman scattering by one LO phonon, the value within the large parentheses in Eq. (6) must be applied for the counting rates of the $Al_xGa_{1-x}As$ sample as well as for that of the Si reference in order to obtain absolute values of the squared Raman polarizability. We used absorption data of Si from Ref. 67, whereas the reflectivity ($r=1-T$) and the refractive index were taken from ellipsometric measurements.[68] The absorption data of GaAs have been reported by Sturge[69] and Sell and Casey[70] ($\alpha=3.0\times10^4$ cm^{-1} at 1.85 eV), its reflectivity and refractive index were selected from ellipsometric measurements.[68] For the $Al_xGa_{1-x}As$ alloy ($x<0.1$) it has been shown that the optical properties above the E_0 gap can be approximated by shifting the values of pure GaAs to account for the increase in the energy of the direct gap $E_0(x)$ with increasing aluminum content x.[5,71,72] Thus, we chose the optical constants to be the same as for GaAs taking the shift of the gap energy $E_0(x)$ as tabulated in Table I into account. We note that n and r obtained in this way compare well with the recent experimental values of Ref. 9.

The Raman scattering intensity can be displayed either as squared Raman polarizability $|\hat{e}_S\cdot\vec{R}\cdot\hat{e}_L|^2$ or as scattering efficiency $dS/d\Omega$. The Raman scattering efficiency includes the ω^4 law and the dependence on the phonon occupation number. It is customary to compare Raman scattering by one and two LO phonons as scattering efficiencies, whereas for Raman scattering by one LO phonon the squared Raman tensors are convenient from the microscopic point of view of Raman polarizabilities. In the case of one-LO-phonon scattering both quantities are related to each other by the expression:[41]

$$\left.\frac{dS}{d\Omega}\right|_{LO}=\frac{\omega_S^3\omega_L}{c^4}\frac{\hbar}{2V_cM^*\Omega_{LO}}\frac{n_S}{n_L}|\hat{e}_S\cdot\vec{R}\cdot\hat{e}_L|^2 \times[1+n(\Omega_{LO})] . \tag{7}$$

We used cw-dye lasers pumped with all lines of an Ar^+ laser to excite the spectra. The dye DCM (Lambda Physik, Göttingen) worked in the range from 1.8 to 2.0 eV, whereas Rhodamine 6G (Lambda Physik, Göttingen) was operated from 1.95 to 2.1 eV. They covered the spectral region close to the $E_0+\Delta_0$ gap of the $Al_xGa_{1-x}As$ ($x<0.1$) systems. The typical power incident on the sample was 200 mW. The power density was kept below 10 W/cm^2 by means of a slit focus to avoid heating. The scattered light was analyzed by a Jarrell-Ash 1-m double monochromator equipped with holographic gratings and was detected with an RCA 31034 photomultiplier by photon counting.

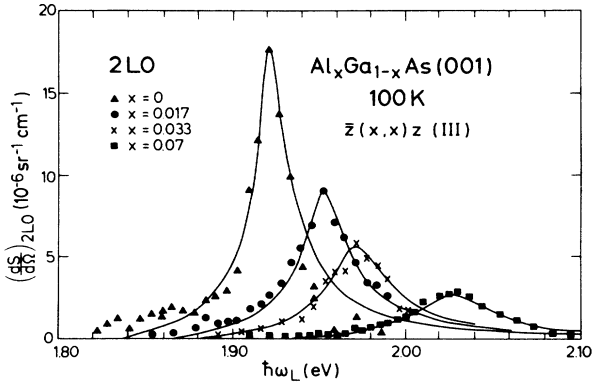

FIG. 1. Efficiencies for Raman scattering by two LO phonons in $Al_xGa_{1-x}As$ at 100 K. The solid lines are fits to the experimental points according to Eqs. (2) and (7) of Ref. 42.

III. RESULTS

Figure 1 depicts the resonance of the efficiency for Raman scattering by two LO phonons near the $E_0+\Delta_0$ gap for the four $Al_xGa_{1-x}As$ samples studied in the composition range $0\leq x\leq0.07$. The solid lines are fits to the experimental points. The $E_0+\Delta_0$ gap increases with higher

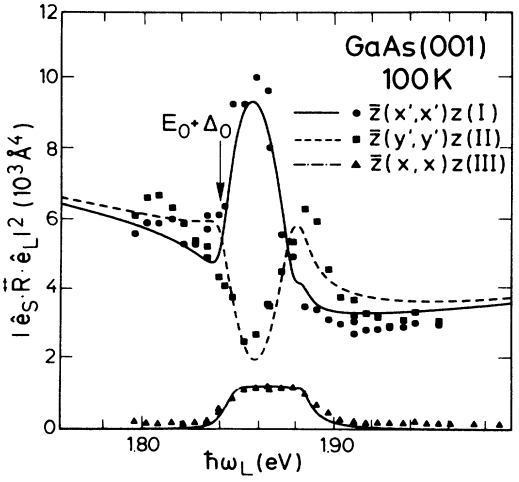

FIG. 2. Squared Raman polarizabilities for scattering by one LO phonon measured on GaAs(001) at 100 K with $\hat{e}_L\|\hat{e}_S$ (configurations I, II, and III). The lines are fits according to Eqs. (4) and (9) of Ref. 43 and Eq. (A1) of Ref. 41.

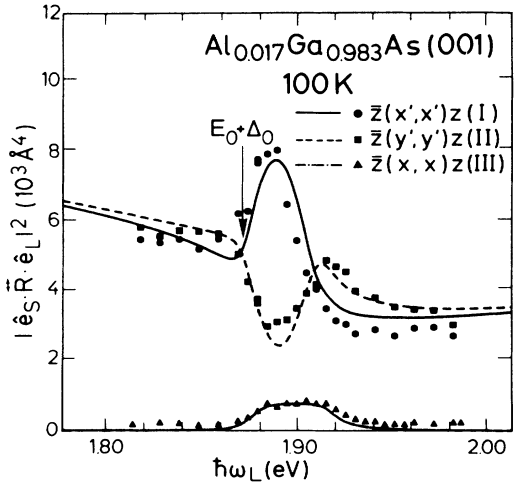

FIG. 3. Squared Raman polarizability for scattering by one LO phonon in $Al_{0.017}Ga_{0.983}As(001)$ measured with $\hat{e}_L \| \hat{e}_S$ (configurations I, II, and III). The lines are fitted according to the theory of Refs. 41 and 43.

aluminum concentration. At the same time the gap considerably broadens. Consequently, the enhancement at the resonance peak decreases as x increases.

Figures 2–4 show the interference of Raman scattering by one LO phonon measured with $\hat{e}_L \| \hat{e}_S$ (configurations I, II, and III) on the $Al_xGa_{1-x}As$ samples with $x=0$, 0.017, and 0.07, respectively. The lines represent theoretical fits. The measurement in configuration IV is omitted in the figures. It shows no detailed resonance close to the $E_0+\Delta_0$ gap and can essentially be represented by an average line between those for the $\bar{z}(x',x')z$ (I) and $\bar{z}(y',y')z$ (II) configurations.

The interference of Raman scattering by LO phonons persists in spite of alloying with aluminum. The shift of the $E_0+\Delta_0$ gap produces a shift of the interference curves

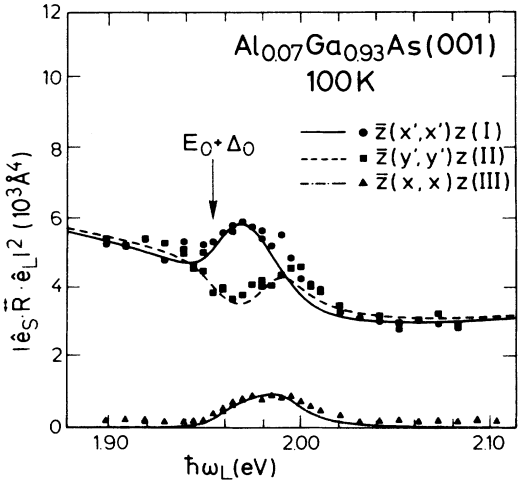

FIG. 4. Squared Raman polarizability for scattering by one LO phonon in $Al_{0.07}Ga_{0.93}As(001)$ measured with $\hat{e}_L \| \hat{e}_S$ (configurations I, II, and III). The lines are fitted according to the theory of Refs. 41 and 43.

to higher laser energies with increasing x. The sharpness of interference and its amplitude decrease with alloying: The dipole-forbidden scattering shows the strongest enhancement in the pure GaAs sample, as was also the case for scattering by two LO phonons. The depth of the destructive interference indicates that a large part of the forbidden scattering is of intrinsic origin. The $Al_xGa_{1-x}As$ samples with $x=0.017$ and $x=0.07$ (Figs. 3 and 4) reveal no apparent difference in the enhancement of the pure dipole-forbidden scattering (configuration III). However, the amplitude of the interference decreases. This feature can be explained by additional broadening and an increasing amount of extrinsic impurity-induced scattering. The dipole-forbidden Raman scattering by one LO phonon is about 5 times lower than the dipole-allowed one. Thus, experimental errors on the strength of the dipole-forbidden contribution are rather large. A detailed line-shape analysis of the resonance of the one-LO-phonon forbidden scattering cannot be reliably made due to the scatter in experimental data.

IV. FITTING PROCEDURE

The theoretical expressions for the resonance of scattering by LO phonons near the $E_0+\Delta_0$ gap that we applied to fit our experimental data are the same as used in Refs. 41–43. The final formula for the scattering efficiency of Raman scattering by two LO phonons is given by Eqs. (2) and (7) of Ref. 42. The two-LO-phonon resonances were fitted first, thus yielding an accurate value for the energy of the $E_0+\Delta_0$ gap and its broadening η from the position and the width of the resonance.[43] A third adjustable parameter served as vertical scale factor which adjusted the calculated Raman scattering efficiencies to those determined experimentally. The vertical factor should, in first approximation, be the same for all calculated Raman scattering efficiencies (independent of composition x). The experimental uncertainties are mainly due to uncertainties in the value of the Raman polarizability of Si which is only known to within 20%.[65]

In order to fit the dipole-allowed Raman scattering by one LO phonon we used the decomposition of the Raman polarizability a_{DP} into contributions from different critical points [Eq. (4) of Ref. 43]: $E_0-E_0+\Delta_0$ (coefficient A_1), $E_1-E_1+\Delta_1$ (A_2), and higher gaps (A_3). Care was taken to describe the behavior of dipole-allowed Raman scattering by LO phonons with the same coefficients A_1, A_2, and A_3 in all $Al_xGa_{1-x}As$ samples studied. The expression of the intrinsic dipole-forbidden scattering by LO phonons is represented by Eqs. (15) and (16) of Ref. 41, whereas the squared Raman polarizability $|a_{Fi}|^2$ for impurity-induced scattering by LO phonons is given in Eq. (A1) of the same paper.

The interference curves were fitted with the energy of the gap $E_0+\Delta_0$ and its broadening η determined from the two-LO-phonon resonance.[43] The prefactor of the calculated resonance curve for the intrinsic and extrinsic dipole-forbidden Raman scattering was adjusted for each contribution to reach the measured resonance peak, assuming the whole scattering intensity is due to that component. Then the relative strength between both was

TABLE II. Parameters of GaAs used with the interpolation scheme proposed by Adachi (Ref. 10).

$\Delta_0=0.34$ eV[a]	$\hbar\Omega_{LO}=36.6$ meV[e]
$E_1=3.028$ eV[b]	$P^2/m=13.8$ eV[f,g]
$E_1+\Delta_1=3.246$ eV[b]	$C_F=2.1\times10^{-5}$ eV cm$^{1/2}$ [h]
$m_e=0.067m$[c]	$a_0=5.65$ Å[i,g]
$m_h=0.16m$[c]	$M^*=66305m$[j]
$q=7.2\times10^5$ cm^{-1} [d]	$x_f=0.06$[k,g]

[a]Reference 73.
[b]Reference 74.
[c]Reference 75.
[d]$q=(n_L\omega_L+n_S\omega_S)/c$.
[e]Reference 76.
[f]$P=\hbar 2\pi/a_0$.
[g]Assumed to be independent of x.
[h]$C_F=[2\pi^2(1/\epsilon_0-1/\epsilon_\infty)\hbar\Omega_{LO}]^{1/2}$.
[i]Reference 77.
[j]$M^*=(1/M_{Ga}+1/M_{As})^{-1}$.
[k]See definition in Ref. 41.

varied so as to fit the observed details of the interference. The relative strength of the interference determines the ratio $|a_F|^2_{max}/(|a_F|^2_{max}+|a_{Fi}|^2_{max})$ of intrinsic dipole-forbidden Raman scattering by LO phonons in the *total* forbidden scattering intensity. The relative amount of intrinsic **q**-induced Raman scattering with respect to the extrinsic impurity-induced one is expressed by the ratio $|a_F|^2_{max}/|a_{Fi}|^2_{max}$.

The material parameters used to evaluate the Raman polarizabilities and scattering efficiencies are summarized in Table II for GaAs. The compositional dependence of these parameters in $Al_xGa_{1-x}As$ was obtained for Table II following the interpolation scheme proposed by Adachi.[10]

V. DISCUSSION

A. Two-phonon resonances

The energy of the band gap $E_0+\Delta_0$ and its broadening η, obtained from the fit of the two-LO-phonon resonances in Fig. 1 (solid lines), are summarized in Table III. The Raman scattering efficiency observed at resonance for $x=0$ amounts to 1.8×10^{-5} sr^{-1}cm^{-1}. The value obtained from fourth-order perturbation theory (0.65×10^{-5} sr^{-1}cm^{-1}) is lower by a factor of 2.5. The same vertical factor has been used for the other resonance curves. The agreement with experiments for all values of x is remarkable. The calculated value of the Raman scattering efficiency for two-LO-phonon scattering has also been found smaller than or equal to the experimental one in InP (Ref. 43) and GaSb (Ref. 44). These differences may be due to uncertainties in input parameters (20% error for the Raman polarizability of Si) and to the neglect of excitonic effects.

1. Compositional dependence of the $E_0+\Delta_0$ gap

Figure 5 shows the compositional dependence of the $E_0+\Delta_0$ gap. Within the composition range we cannot observe a deviation from a linear dependence. The solid line in Fig. 5 corresponds to ($x\leq0.1$)

$$E_0+\Delta_0(x)=1.847+1.56x \text{ eV} . \quad (8)$$

The experimental data on the compositional change of the $E_0+\Delta_0$ gap in $Al_xGa_{1-x}As$ were mostly obtained for samples with aluminum concentration $x\geq0.10$ at room temperature.[5,7,9] The dependence established for $E_0+\Delta_0$, if one takes a temperature shift of 80 meV into account, corresponds to the dot-dashed line of Fig. 5 [$E_0+\Delta_0(x)=1.845+1.115x+0.37x^2$ eV].[7] Casey's dependence of the E_0 gap [Eq. (1)],[11] shifted by $\Delta_0=330$ meV, is represented by the dashed line in Fig. 5. The linear dependence determined by Monemar *et al.*[5] nearly coincides with our solid line. Recently, Aspnes *et al.*[9] proposed a third-order dependence on composition for the E_0 gap at room temperature. The dot-dot-dashed line depicts their data shifted by 421 meV to account for Δ_0 and the temperature difference [$E_0+\Delta_0(x)=1.845+1.594x+x(1-x)(0.127+1.319x)$ eV]. The best agreement with our data is found for the linear dependence given in Ref. 5. However, this agreement deteriorates if we determine the alloy composition x from the E_0 luminescence (see Sec. II) using Monemar's or Aspnes's relation.[5,9] This observation suggests that the gap that enters the resonance

TABLE III. Parameters obtained from the fit of the two-LO-phonon resonance curves and one-LO-phonon interference curves.

	Sample			
	1	2	3	4
Al concentration (at. %)	0	1.7±0.3	3.3±0.3	7.0±0.5
$E_0+\Delta_0$ (eV)	1.845±0.003	1.875±0.003	1.899±0.003	1.955±0.003
η (meV)	3.5±0.5	6±0.5	8±0.5	12±1
A_1 (Å^2)	8	8	7	7.5
A_2 (Å^2)	26	26	26	23
A_3 (Å^2)	−3	−6	−3	−3
$\lvert a_F\rvert^2_{max}$ (Å^4)	0.77×10^3	0.41×10^3	0.16×10^3	0.09×10^3
$\lvert a_{Fi}\rvert^2_{max}$ (Å^4)	1.02×10^3	0.58×10^3	0.74×10^3	0.91×10^3
$\frac{\lvert a_F\rvert^2_{max}}{\lvert a_{Fi}\rvert^2_{max}}$	0.75	0.71	0.22	0.10
$\frac{\lvert a_F\rvert^2_{max}}{\lvert a_F\rvert^2_{max}+\lvert a_{Fi}\rvert^2_{max}}$	43%	40%	18%	9%

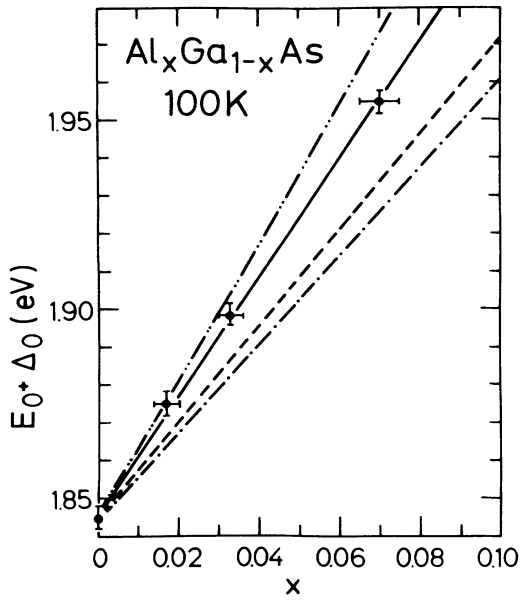

FIG. 5. Compositional dependence of the $E_0+\Delta_0$ gap in $Al_xGa_{1-x}As$ ($x \leq 0.07$). The solid line represents a linear fit according to Eq. (8); the dashed, dot-dashed, and dot-dot-dashed lines correspond to compositional dependences found in the literature (Refs. 11, 7, and 9, respectively).

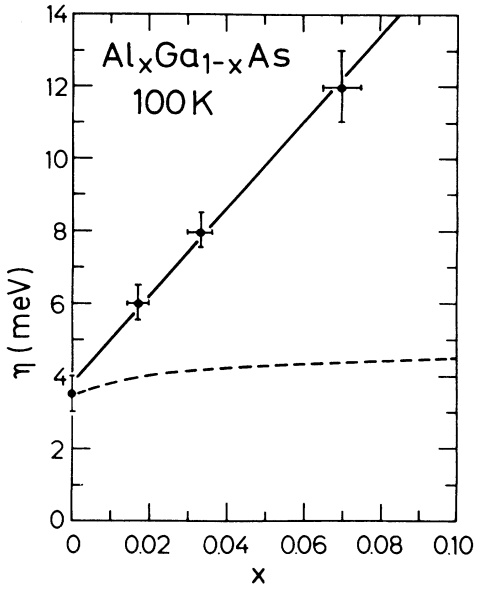

FIG. 6. Compositional dependence of the broadening η of the $E_0+\Delta_0$ gap in $Al_xGa_{1-x}As$ ($x \leq 0.07$). The solid line represents a linear fit according to Eq. (9). The dashed line depicts the gap broadening calculated from Eq. (20).

of Raman scattering efficiencies may differ from that obtained from photoluminescence. In the case of Raman scattering it has already been pointed out that different processes may resonate at slightly different gaps.[43,78,79]

For pure GaAs, the energy obtained for the $E_0+\Delta_0$ gap at 100 K ($=1.845\pm0.003$ eV) is found to agree with a value derived from ellipsometric measurements at 80 K (1.841 ± 0.003 eV).[80]

2. *Compositional dependence of* η

Figure 6 shows the dependence of the Lorentzian broadening η of the $E_0+\Delta_0$ gap on x. Within the experimental error η varies linearly with x ($x \leq 0.07$):

$$\eta(x)=3.8+120x \text{ meV} . \tag{9}$$

A fitted line which assumes a $x(1-x)$ dependence according to binominal statistics would only show small deviations from the solid line in Fig. 6 within the composition range under investigation.

The intrinsic broadening found for GaAs amounts to about 3.5 meV. Alloying considerably increases this broadening. We will apply two theoretical approaches in an attempt to elucidate the nature of the broadening.

First, let us consider the intrinsic broadening of GaAs ($\eta=3.5$ meV). It is lower than that found experimentally by reflectance ($\eta=10$ meV),[81] magnetoreflectance ($\eta=11$ meV),[82] and electroreflectance ($\eta=6\pm2$ meV).[73] A similar discrepancy has been observed in InP ($\eta=5$ versus 10 meV).[43] The Lorentzian broadening of the $E_0+\Delta_0$ gap is larger than for the E_0 gap [the latter is less than 2 meV (Ref. 83)]. This is due to the fact that holes in the split-off band near the Γ point have more decay channels than holes in the light-hole and heavy-hole bands. Thus, the broadening of the $E_0+\Delta_0$ gap is essentially determined by the lifetime of the hole in the split-off band. In pure GaAs at low temperature, the hole state in the split-off band decays into the light-hole and heavy-hole bands mainly by emission of an optical phonon.[84] Neglecting multiple coupling of phonons to electrons, the intrinsic broadening can be directly related to the optical deformation potential d_0 following the analysis of Lawaetz:[84]

$$\eta=\zeta_1 d_0^2+\zeta_p a_p^2 . \tag{10}$$

$\zeta_1 d_0^2$ describes the broadening due to the nonpolar deformation-potential interaction, whereas $\zeta_p a_p^2$ accounts for the polar coupling due to the Fröhlich interaction. ζ_1 and ζ_p are weighting factors which take the **k**-space integration of the density of states into account. For GaAs (with $\zeta_1=5\times10^{-6}$ eV^{-1}) $\zeta_p a_p^2$ amounts to 1.5 meV.[84] The deformation-potential contribution then becomes 2 meV, which corresponds to an optical deformation potential d_0 equal to 20 eV. This value is nearly one-half that generally accepted. Calculations with the nonlocal empirical-pseudopotential method (EPM) yield 36 eV in agreement with results from the sp^3 model of the LCAO method.[85] Both values can be compared with $d_0=48$ eV determined from resonant Raman scattering[64] and $d_0=41$ eV found with Eq. (10) for $\eta=10$ meV as obtained from reflectance measurements.[81,84] Although there is a large spread for the values of d_0, a value between 30–45 eV is generally accepted. As in InP,[43] the deformation potential which results from the broadening of the $E_0+\Delta_0$ gap by the resonance of two-LO-phonon Raman scattering turns out to be too low by a factor of 2. The linear muffin-tin-orbital method (LMTO) and the sp^3s^* model of the LCAO approach yield, however, rather low deformation

potentials, which are in better agreement with the value obtained here: LMTO, $d_0=18$ eV;[85] sp^3s^* LCAO, $d_0=21$ eV.[86] A slightly higher deformation potential $d_0=23$ eV is obtained by *ab initio* pseudopotential calculations.[87,88] A similar discrepancy between the deformation potentials calculated by the EPM (Ref. 20) and LMTO (Refs. 86, 89, and 90) method also exist in InP, Si, and CdTe. Very recently, however, Brey *et al.* have shown that the discrepancy is due to the charge symmetrization procedure inherent to the LMTO method. Correction of this problem leads to $d_0=25.1$ eV for GaAs within the LMTO method.[91] This fact suggests that the resonance profile of LO-phonon scattering may be sharpened by excitonic effects at the $E_0+\Delta_0$ gap.

In the $Al_xGa_{1-x}As$ alloys the gap is additionally broadened due to the different cation potentials of the aluminum and gallium atoms. The wave functions of the hole states in the valence band are essentially built up by the p functions of the cation.[92–96] Thus, the valence-band states are more strongly affected by alloying than the conduction-band states. The difference in the cation potentials and the band mixing between the light-hole band and the split-off band lead to a scattering of the hole state from the split-off band into the light-hole band. For reasons of simplicity we neglect scattering from the split-off into the heavy-hole band because of the near orthogonality of the wave functions. This simple model for the broadening η can be treated quantitatively using Fermi's golden rule and applying results from $\mathbf{k}\cdot\mathbf{p}$ and tight-binding calculations:[92–94]

$$\eta\simeq\Delta E=2\pi\,|\,W_{fi}\,|^2 n(-\Delta_0)\ . \tag{11}$$

In Eq. (11) ΔE is the energy uncertainty, W_{fi} the perturbation matrix element, and $n(-\Delta_0)$ the density of states in the light-hole band at the energy of the spin-orbit splitting Δ_0 (the origin of energies is chosen to be the top of the valence band). The density of states (for one spin orientation) is given by the expression:

$$n(-\Delta_0)=-\frac{V}{2\pi^2}k_0^2\left|\frac{\partial E}{\partial k}\right|^{-1}_{\mathbf{k}=\mathbf{k}_0}\ , \tag{12}$$

where V is the crystal volume, $\mathbf{k}_0$ the wave vector at which the kinetic energy of the light hole equals Δ_0. $\mathbf{k}\cdot\mathbf{p}$ calculations including higher conduction bands yield $|\,\mathbf{k}_0\,|=1.38\times10^6$ cm^{-1} and $|\,\partial E/\partial k\,|_{\mathbf{k}=\mathbf{k}_0}=2.55\times10^8$ eV cm.[97] The perturbation matrix element can be approximated by[92]

$$|\,W_{fi}\,|^2=x\frac{V_c}{V}\,|\,E_p(\mathrm{Ga})-E_p(\mathrm{Al})\,|^2\gamma^2\beta^2\ . \tag{13}$$

x is the Al concentration and gives the probability of finding an Al atom on a Ga site per unit cell. E_p(Ga) and E_p(Al) are the diagonal matrix elements of the p functions of the Ga and Al atoms [$E_p(\mathrm{Ga})-E_p(\mathrm{Al})\simeq0.04$ (Refs. 92 and 93) or 0.08 eV (Ref. 94)]. γ denotes the band admixture of the split-off hole state of the Γ point in the light-hole band at the point $\mathbf{k}_0$ (at $E=-\Delta_0$, $\gamma=1/\sqrt{3}$ from $\mathbf{k}\cdot\mathbf{p}$ theory).[98] β accounts for the contribution of a cationlike p function to the valence-band states ($\beta\simeq0.39$ from tight-binding calculations).[92] The prefactor V_c/V considers the fact that $x\,|\,E_p(\mathrm{Ga})-E_p(\mathrm{Al})\,|^2\gamma^2\beta^2$ yields the squared perturbation matrix element per unit cell, whereas the density of states $n(E)$ refers to the total crystal volume. With the volume of the primitive cell $V_c=a_0^3/4$ and the parameters given by Harrison[92] one obtains the linear compositional dependence of the broadening:

$$\eta\simeq3.4\times10^{-5}x\ \text{eV}\ . \tag{14}$$

It becomes 4 times larger for the $E_p(\mathrm{Ga})-E_p(\mathrm{Al})$ of Vogl *et al.*[94] Expression (14) yields broadenings of the order of μeV's which are 3 orders of magnitude lower than the experimental one. This small value of η results from the small mixing of cation wave functions in the valence bands and from the near orthogonality of the split-off and heavy-hole functions. It is thus very difficult to enhance the value of η obtained within this model.

The spread of the gap energy $E_0+\Delta_0$ due to the fluctuations in alloy composition (inhomogeneous broadening) can be estimated from a model proposed by Schubert *et al.*[99] The model has been successfully applied to the alloy broadening observed in photoluminescence spectra of $Al_xGa_{1-x}As$. It assumes that the Al and Ga atoms are randomly distributed on the cation sites in an ideal crystal. It does not account for macroscopic inhomogeneities such as clustering.

The probability of finding n Al atoms within a volume V^* is given by binominal statistics (Bernoulli distribution):[98,99]

$$p(n)=\binom{\rho V^*}{n}x^n(1-x)^{\rho V^*-n}\ . \tag{15}$$

$\rho=4/a_0^3$ is the cation density (2.2×10^{22} cm^{-3}). V^* denotes the volume relevant for the Raman process. The mean value of the distribution is $\bar{n}=\rho V^*x$ and the variance $\sigma_n^2=\rho V^*x(1-x)$.[100] The standard deviation of the alloy composition x within the probing volume V^* becomes[99,100]

$$\sigma_x=\sigma_n/\rho V^*=\left[\frac{x(1-x)}{\rho V^*}\right]^{1/2}\ . \tag{16}$$

The standard deviation of the band-gap energy is obtained by combining Eq. (16) with the dependence of the band gap on composition [Eq. (8)]:[99]

$$\sigma_E=\frac{d(E_0+\Delta_0)}{dx}\sigma_x=1.6\sigma_x\ \text{eV}\ . \tag{17}$$

The fluctuations in alloy composition will appear as an additional "inhomogeneous" broadening in the resonance curves.

The numerical evaluation of Eq. (17) requires an estimate of the minimum scattering volume V^*. If the intermediate states in the scattering process were excitons, we may take for V^* the excitonic volume:

$$V^*_{\mathrm{ex}}=\frac{4\pi}{3}a_B^3=\frac{4\pi}{3}\left[\frac{\hbar^2\epsilon_0}{\mu e^2}\right]^3 \tag{18}$$

with the Bohr radius $a_B = 140$ Å for GaAs, ϵ_0 the low frequency (rf) dielectric constant, μ the reduced electron mass, and e the free-electron charge.

From Eqs. (16) and (17) we obtain

$$\eta = 3.4[x(1-x)]^{1/2} \text{ meV} . \quad (19)$$

This function is plotted as a dashed line in Fig. 6. It gives a broadening nearly an order of magnitude smaller than the observed one. We note that Eq. (19) accounts well for the broadening of the edge luminescence (E_0) of $Al_xGa_{1-x}As$.[99] Hence the failure to do so for $E_0+\Delta_0$ may be related to the larger density of scattering channels associated with $E_0+\Delta_0$. Nonspherically symmetric defects, such as Al-Al pairs in nearest- or second-nearest-neighbor positions, or other types of clusters, would enhance considerably the scattering to the top valence bands and also involve the heavy-hole band with its large density of states. On the other hand, the broadening of the $E_0+\Delta_0$ gap may be partly due to the suppression of excitonic effects with alloying. This point deserves further investigation.

B. One-LO-phonon interference curves

The fits of the interference curves depicted in Figs. 2–4 and the determination of the impurity-induced contribution to the scattering by LO phonons provides a further tool to study the effects of the Al atoms in the GaAs matrix. It is, however, difficult to separate *quantitatively* the influence of alloying with Al on the impurity-induced Raman scattering from that of contaminants added with Al to the melt.

1. *Dipole-allowed Raman scattering by LO phonons*

The fit of the dipole-allowed deformation-potential-induced Raman scattering by LO phonons with Eq. (4) of Ref. 43 yields the coefficients of the contributions from the different gaps independent of alloy composition x within the experimental error: $E_0-E_0+\Delta_0$ gap, $A_1 = 7.5 \pm 0.5$ Å^2; $E_1-E_1+\Delta_1$ gap, $A_2 = 25 \pm 3$ Å^2; higher gaps, $A_3 = -5 \pm 5$ Å^2. The relative signs and magnitude of the coefficients are the same as in the fits previously reported for pure GaAs,[41,64] except for A_2 in Ref. 64. The coefficient A_1 can be related to the optical deformation potential d_0 of the $E_0-E_0+\Delta_0$ gap:[38,43,64]

$$A_1 = \frac{\sqrt{3}}{128\pi}\frac{a_0^2}{E_0}C_0''d_0 . \quad (20)$$

where a_0 is the lattice constant, E_0 the gap energy, and C_0'' a constant which can be deduced from the piezobirefringence for a [111] stress.[95] We obtain $C_0''d_0 = 87.2$ eV. The determination of d_0 requires a value for C_0'' which is only known with large uncertainties (1.5–2.5).[101] We thus derive d_0 between 35–58 eV, which agrees within error with the value generally accepted [$d_0 = 30$–45 eV (Refs. 84 and 86)].

The coefficient A_2 is related to the two- ($d_{1,0}^5$) and three-band ($d_{3,0}^5$) optical deformation potentials at the $E_1-E_1+\Delta_1$ gap through (in atomic units $e=\hbar=m=1$):[38,64,102]

$$A_2 = \frac{\sqrt{2}a_0}{9\pi E_1^2}\left[d_{3,0}^5 + \frac{1}{2\sqrt{2}}d_{1,0}^5\right] , \quad (21)$$

where E_1 is the gap energy. With Eq. (21) and $A_2 = 25$ Å we find $d_{3,0}^5 + (1/2\sqrt{2})d_{1,0}^5$ equal 58 eV. This value, obtained from the fit of the dipole-allowed Raman scattering near the $E_0+\Delta_0$ gap (Figs. 2–4), is somewhat larger than that determined from the resonant scattering around the E_1 gap (37 eV).[64] Pseudopotential calculations yield for this number 32 eV ($d_{3,0}^5 = 38$ eV and $d_{1,0}^5 = -19$ eV).[103] A similar discrepancy between calculated optical deformation potentials and those determined from the fit of Raman resonance curves has been pointed out for GaSb.[44] It may be mainly due to a large uncertainty in the extrapolation of the $E_1-E_1+\Delta_1$ contribution to the region near the $E_0+\Delta_0$ gap.

2. *Interference curves and dipole-forbidden scattering by LO phonons*

The real and imaginary parts of the Raman polarizability a_{DP} and a_F for dipole-allowed and dipole-forbidden Raman scattering by LO phonons as obtained from the fit of Fig. 2 in GaAs, are depicted in Fig. 7. The decrease in broadening of the $E_0+\Delta_0$ gap for the fit of Fig. 2 ($\eta = 3.5$ meV) with respect to Fig. 2 of Ref. 41 ($\eta = 8$ meV) improves only slightly the fit (mainly at $\hbar\omega_L = E_0+\Delta_0 + \hbar\Omega_{LO}$, configuration II), while the fit to the two-LO-phonon resonance requires much more stringently $\eta = 3.5$ meV (see Sec. V A). Hence, we suggest that the fitting procedure for $E_0+\Delta_0$ resonances should start at the two-LO-phonon resonance and use the values of η and $E_0+\Delta_0$ so obtained for all other fits. The best fit in Fig. 2 is obtained for $|a_F|^2/|a_{Fi}|^2 = 0.75$, which means that about 43% of the total dipole-forbidden Raman scattering is due to the intrinsic q-induced Fröhlich mechanism. This result differs somewhat from that of Ref. 41 on a

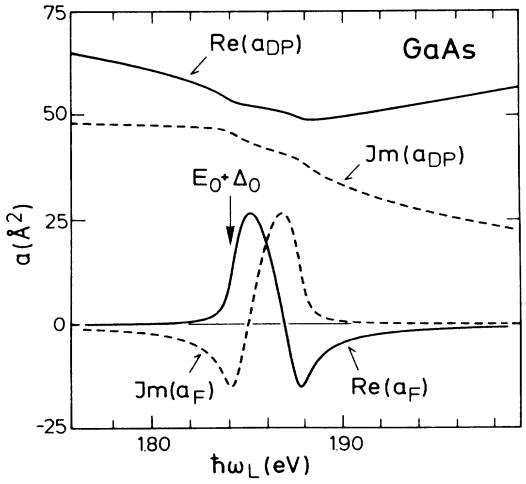

FIG. 7. Energy dependence of the Raman polarizabilities a_{DP} for LO-phonon dipole-allowed [Eq. (4) of Ref. 43] and a_F for LO-phonon intrinsic dipole-forbidden scattering [Eq. (9) of Ref. 43] calculated with the parameters of Table II for the fit of Fig. 2 on pure GaAs.

similar sample calculated with a larger broadening. Although the interferences observed in both samples are very similar (compare Fig. 2 of Ref. 41 with Fig. 2 of this paper) a fit in Ref. 41 with $\eta=8$ meV yields that only 30% of the total scattering efficiency is of intrinsic origin. A value of 43% intrinsic Fröhlich-induced scattering compares very well with 40% also found in high-purity InP.[43] Thus even in high-purity epitaxial samples the main forbidden contribution to LO-phonon scattering is impurity induced. The estimated error in the percentage of intrinsic scattering is 5%.

When the Al content amounts to $x=0.017$ (sample 2), the interference persists with the same sign, while the dipole-forbidden Raman scattering decreases slightly together with the height of the interference (Fig. 3). This effect can be related to the broadening of the $E_0+\Delta_0$ gap (change from 3.5 meV to 6 meV). For the fit in Fig. 3, the impurity-induced contribution has been increased by 5% with respect to the intrinsic contribution ($|a_F|^2_{\max}/|a_{Fi}|^2_{\max}=0.71$). This increase, although it may suggest the expected trend, is below the estimated error. It reveals that high-quality $Al_xGa_{1-x}As$ samples, comparable to pure epitaxial GaAs, can be grown by liquid-phase epitaxy. Although the crystal contains about 3.3×10^{20} cm^{-3} Al atoms the impurity-induced Raman scattering remains nearly the same which is contrary to the observation in bulk GaAs with $N_A+N_D\simeq10^{16}$ cm^{-3}.[41] The atomic potential of the Al ions is rather similar to that of the Ga ions,[89] and the Al ions are very far from playing the role of (ionized) impurities required in the fourth-order process for impurity-induced Raman scattering by LO phonons.

On the other hand, the impurity-induced scattering becomes larger as one increases the aluminum content even further. In sample 3, with $x=0.033$, the Fröhlich-induced Raman scattering by LO phonons contributes with about 18% to the total scattering intensity, for $x=0.07$ (sample 4) it decreases further to about 9% (see Table III and Fig. 4). The total efficiency for dipole-forbidden scattering by LO phonons remains almost constant from $x=0.017$ (sample 2, Fig. 3) to $x=0.07$ (sample 4, Fig. 4) although the broadening of the $E_0+\Delta_0$ gap is doubled (from 6 to 12 meV), thus revealing that the effective ionized-impurity concentration must increase. Quantitative estimates of the scattering efficiencies [prefactor of Eq. (A1) in Ref. 41] require a relative increase of n_I by 6.5 to enhance the squared Raman polarizability for impurity-induced scattering $|a_{Fi}|^2_{\max}$ from 580 Å in sample 2 to 910 Å in sample 4 (Table III). This value is in satisfactory agreement with the ionized-impurity concentrations deduced from mobility measurements at 77 K (10 times larger in sample 2 than in sample 4).

VI. CONCLUSION

We have shown that the interference of dipole-allowed and dipole-forbidden Raman scattering by LO phonons near the $E_0+\Delta_0$ gap persists in liquid-phase epitaxy samples when aluminum is added to GaAs in the melt. The aluminum concentration, however, shifts and broadens the gap. The $E_0+\Delta_0$ gap as well as its broadening η show a linear dependence on the alloy composition x within the small aluminum concentration range under investigation ($x\leq0.07$). Estimates for the variation of the gap broadening with aluminum content lead to the conclusion that inhomogeneous broadening, effects of cluster formation, and impurities other than the Al may play an important role.

ACKNOWLEDGMENTS

We gratefully acknowledge the technical assistance of H. Hirt, M. Siemers, and P. Wurster. Thanks are due to B. Kunath for the sample growth and characterization and to K. Kelting for performing the luminescence measurements. We also thank V. Vorlíček for a critical reading of the manuscript.

[1]S. M. Ku and J. F. Black, J. Appl. Phys. **37**, 3733 (1966).
[2]J. F. Black and S. M. Ku, J. Electrochem. Soc. **113**, 240 (1966).
[3]M. B. Panish and S. Sumski, J. Phys. Chem. Solids **30**, 129 (1969).
[4]H. Neumann and W. Junge, Phys. Status Solidi A **34**, K39 (1976).
[5]B. Monemar, K. K. Shih, and G. D. Pettit, J. Appl. Phys. **47**, 2604 (1976).
[6]A. Y. Cho and S. E. Stokowski, Solid State Commun. **9**, 565 (1971).
[7]O. Berolo and J. C. Woolley, Can. J. Phys. **49**, 1335 (1971); O. Berolo and J. C. Woolley, in *Proceedings of the Eleventh International Conference on the Physics of Semiconductors, Warsaw, 1972* (Polish Scientific Publishers, Warsaw, 1972), p. 1420.
[8]B. A. Boleylev, Kh. B. Zembatov, A. F. Kravchenko, and Yu. V. Lobuvets, Izv. Vuzov. Fiz. **6**, 113 (1974).
[9]D. E. Aspnes, S. M. Kelso, R. A. Logan, and R. Bhat, J. Appl. Phys. **60**, 754 (1986).
[10]S. Adachi, J. Appl. Phys. **58**, R1 (1985).
[11]H. C. Casey and M. B. Panish, *Heterostructure Lasers* (Academic, New York, 1978), Part B.
[12]H. J. Lee, L. Y. Juravel, and J. C. Woolley, Phys. Rev. B **21**, 659 (1980).
[13]L. Nordheim, Ann. Phys. (Leipzig) **9**, 607 (1931); **9**, 641 (1931).
[14]J. C. Phillips, *Bonds and Bands in Semiconductors* (Academic, New York, 1973).
[15]K.-R. Schulze, H. Neumann, and K. Unger, Phys. Status Solidi B **75**, 493 (1976).
[16]A. Baldereschi, E. Hess, K. Maschke, H. Neumann, K.-R. Schulze, and K. Unger, J. Phys. C **10**, 4709 (1977).
[17]D. Stroud and H. Ehrenreich, Phys. Rev. B **2**, 3197 (1970).
[18]E. D. Siggia, Phys. Rev. B **10**, 5147 (1974).
[19]A.-B. Chen and A. Sher, Phys. Rev. B **22**, 3886 (1980).
[20]A.-B. Chen and A. Sher, Phys. Rev. B **23**, 5645 (1981).
[21]D. J. Chadi and M. L. Cohen, Phys. Rev. B **7**, 692 (1973).
[22]K. C. Hass, H. Ehrenreich, and B. Velicky, Phys. Rev. B **27**, 1088 (1983).
[23]A.-B. Chen and A. Sher, Phys. Rev. B **17**, 4726 (1978).
[24]A.-B. Chen and A. Sher, Phys. Rev. B **23**, 5360 (1981).
[25]N. Holonyak, Jr., W. D. Laidig, and B. A. Vojak, Phys. Rev.

Lett. **45**, 1703 (1980).
[26]T. S. Kuan, T. F. Kuech, W. I. Wang, and E. L. Wilkie, Phys. Rev. Lett. **54**, 201 (1985).
[27]N. E. Christensen, E. Molinari, and G. B. Bachelet, Solid State Commun. **56**, 125 (1985).
[28]A. Balzarotti, P. Letardi, and N. Motta, Solid State Commun. **56**, 471 (1985).
[29]O. G. Lorimor and W. G. Spitzer, J. Appl. Phys. **37**, 2509 (1966).
[30]M. Ilegems and P. L. Pearson, Phys. Rev. B **1**, 1576 (1970).
[31]J. Shah, A. E. DiGiovanni, T. C. Damen, and B. I. Miller, Phys. Rev. B **7**, 3481 (1973).
[32]O. K. Kim and W. G. Spitzer, J. Appl. Phys. **50**, 4362 (1979).
[33]B. Jusserand and J. Sapriel, Phys. Rev. B **24**, 7194 (1981).
[34]H. Kawamura, R. Tsu, and L. Esaki, Phys. Rev. Lett. **29**, 1397 (1972).
[35]D. N. Talwar, M. Vandevyver, and M. Zigone, Phys. Rev. B **23**, 1743 (1981).
[36]N. Saint-Cricq, R. Carles, J. B. Renucci, A. Zwick, and M. A. Renucci, Solid State Commun. **39**, 1137 (1981).
[37]W. Richter, in *Solid State Physics*, Vol. 78 of *Springer Tracts in Modern Physics*, edited by G. Höhler (Springer, Berlin, 1976), p. 121.
[38]M. Cardona, in *Light Scattering in Solids II*, Vol. 50 of *Topics in Applied Physics*, edited by M. Cardona and G. Güntherodt (Springer, Berlin, 1982), p. 19.
[39]P. Vogl, in *Physics of Nonlinear Transport in Semiconductors*, edited by D. K. Ferry, J. R. Barker, and C. Jacoboni (Plenum, New York, 1980), p. 75.
[40]J. Menéndez and M. Cardona, Phys. Rev. Lett. **51**, 1297 (1983).
[41]J. Menéndez and M. Cardona, Phys. Rev. B **31**, 3696 (1985).
[42]J. Menéndez, M. Cardona, and L. K. Vodopyanov, Phys. Rev. B **31**, 3705 (1985).
[43]W. Kauschke and M. Cardona, Phys. Rev. B **33**, 5473 (1986).
[44]W. Kauschke and M. Cardona, Phys. Rev. B (to be published).
[45]R. M. Martin, Phys. Rev. B **4**, 3676 (1971).
[46]R. Zeyher, C.-S. Ting, and J. L. Birman, Phys. Rev. B **10**, 1725 (1974).
[47]D. C. Hamilton, Phys. Rev. **188**, 1221 (1969).
[48]R. M. Martin and T. C. Damen, Phys. Rev. Lett. **26**, 86 (1971).
[49]S. Permogorov and A. Reznitsky, Solid State Commun. **18**, 781 (1970).
[50]R. Trommer and M. Cardona, Phys. Rev. B **17**, 1865 (1978).
[51]P. J. Colwell and M. V. Klein, Solid State Commun. **8**, 2095 (1970).
[52]A. A. Gogolin and E. I. Rashba, in *Proceedings of the 13th International Conference on the Physics of Semiconductors, Rome, 1976*, edited by F. G. Fumi (Tipographia Marves, Rome, 1976), p. 284.
[53]A. A. Gogolin and E. I. Rashba, Solid State Commun. **19**, 1177 (1976).
[54]R. Zeyher, Phys. Rev. B **9**, 4439 (1974).
[55]A. A. Klochikhin and A. G. Plyukhin, Pis'ma Zh. Eksp. Teor. Fiz. **21**, 265 (1975) [JETP Lett. **21**, 122 (1975)].
[56]A. A. Klochikhin, S. A. Permogorov, and A. N. Reznitskii, Zh. Eksp. Teor. Fiz. **71**, 2230 (1976) [Sov. Phys.—JETP **44**, 1176 (1976)].
[57]A. A. Abdumalikov and A. A. Klochikhin, Phys. Status Solidi B **80**, 43 (1977).
[58]A. A. Klochikhin, Ya. V. Morozenko, and S. A. Permogorov, Fiz. Tverd. Tela (Leningrad) **20**, 355 (1978) [Sov. Phys.—Solid State **20**, 2057 (1978)].
[59]C. T. Giner, I. G. Lang, and S. T. Pavlov, Zh. Eksp. Teor. Fiz. **87**, 898 (1984) [Sov. Phys.—JETP **60**, 510 (1984)].
[60]R. G. Ulbrich and C. Weisbuch, Phys. Rev. Lett. **38**, 865 (1977).
[61]E. F. Schubert and K. Ploog, J. Phys. C **18**, 4549 (1985).
[62]V. Swaminathan, J. L. Zilko, W. T. Tsang, and W. R. Wagner, J. Appl. Phys. **53**, 5163 (1982).
[63]H. C. Gatos and M. C. Lavine, in *Progress in Semiconductors*, edited by A. F. Gibson and R. E. Burgess (Temple, London, 1965), Vol. 9, p. 1.
[64]M. H. Grimsditch, D. Olego, and M. Cardona, Phys. Rev. B **20**, 1758 (1979).
[65]J. Wagner and M. Cardona, Solid State Commun. **48**, 301 (1983).
[66]H. Wendel, Solid State Commun. **31**, 423 (1979).
[67]W. C. Dash and R. Newman, Phys. Rev. **99**, 1151 (1955).
[68]D. E. Aspnes and A. A. Studna, Phys. Rev. B **27**, 985 (1983).
[69]M. D. Sturge, Phys. Rev. **127**, 768 (1962).
[70]D. D. Sell and H. C. Casey, J. Appl. Phys. **45**, 800 (1974).
[71]H. C. Casey, Jr., D. D. Sell, and M. B. Panish, Appl. Phys. Lett. **24**, 63 (1974).
[72]H. S. Sommers, Jr. and H. F. Lockwood, J. Appl. Phys. **48**, 4000 (1977).
[73]D. E. Aspnes and A. A. Studna, Phys. Rev. B **7**, 4605 (1973).
[74]S. O. Sari and S. E. Schnatterly, Surf. Sci. **37**, 328 (1973).
[75]Q. H. F. Vrehen, J. Phys. Chem. Solids **29**, 129 (1968).
[76]J. S. Blakemore, J. Appl. Phys. **53**, R123 (1982).
[77]C. M. H. Driscoll, A. F. W. Willoughby, J. B. Mullin, and B. W. Straughan, *Gallium Arsenide and Related Compounds*, Inst. Phys. Conf. Ser. **24**, edited by J. Bok (IOP, Bristol, 1975), p. 275.
[78]M. A. Renucci, J. B. Renucci, R. Zeyher, and M. Cardona, Phys. Rev. B **10**, 4309 (1974).
[79]W. Kiefer, W. Richter, and M. Cardona, Phys. Rev. B **12**, 2346 (1975).
[80]P. Lautenschlager, M. Garriga, S. Logothetidis, and M. Cardona, Phys. Rev. B (to be published).
[81]D. D. Sell and S. E. Stokowski, in *Proceedings of the 10th International Conference on the Physics of Semiconductors, Cambridge, Mass., 1970*, edited by S. P. Keller, J. C. Hensel, and F. Stern (USAEC, Oak Ridge, 1970), p. 417.
[82]M. Reine, R. L. Aggarwal, B. Lax, and C. M. Wolfe, Phys. Rev. B **2**, 458 (1970).
[83]A. K. Sood, W. Kauschke, J. Menéndez, and M. Cardona, Phys. Rev. B **35**, 2886 (1987).
[84]P. Lawaetz, D. Sc. thesis, The Technical University of Denmark, Lyngby, 1978.
[85]N. E. Christensen, Phys. Rev. B **30**, 5753 (1984).
[86]A. Blacha, H. Presting, and M. Cardona, Phys. Status Solidi B **126**, 11 (1984).
[87]O. H. Nielson and R. M. Martin, Phys. Rev. B **32**, 3792 (1985).
[88]O. H. Nielson (private communication).
[89]N. E. Christensen, Solid State Commun. **50**, 177 (1984).
[90]N. E. Christensen (private communication).
[91]L. Brey, N. E. Christensen, and M. Cardona (unpublished).
[92]W. A. Harrison, *Electronic Structure and Properties of Solids* (Freeman, San Fransisco, 1982).
[93]W. A. Harrison, Phys. Rev. B **24**, 5835 (1981).
[94]P. Vogl, H. P. Hjalmarson, and J. D. Dow, J. Phys. Chem. Solids **44**, 365 (1983).
[95]M. Cardona, in *Atomic Structure and Properties of Solids* Proceedings of the International School in Physics "Enrico Fermi," Course 52, Narenna, Italy, 1971, edited by E. Bur-

stein (Academic, New York, 1972), p. 514.
[96]M. Cardona, J. Phys. Chem. Solids **24**, 104 (1963).
[97]G. Fasol (private communication).
[98]E. O. Kane, J. Phys. Chem. Solids **1**, 249 (1957).
[99]E. F. Schubert, E. O. Göbel, Y. Horikoshi, K. Ploog, and H. J. Queisser, Phys. Rev. B **30**, 813 (1984).
[100]J. Mathews and R. L. Walker, *Mathematical Methods of Physics* (Benjamin, New York, 1970).
[101]C. W. Higginbotham, M. Cardona, and F. H. Pollak, Phys. Rev. **184**, 821 (1969).
[102]A. K. Sood, G. Contreras, and M. Cardona, Phys. Rev. B **31**, 3760 (1985).
[103]H. Presting, Ph.D. thesis, Stuttgart, 1985 (unpubilshed).